Miniaturized Fully-Passive Brain Implant for Wireless Neuropotential Acquisition

Cedric W. L. Lee, *Student Member, IEEE*, Asimina Kiourti, *Member, IEEE* and John L. Volakis, *Fellow, IEEE*

***Abstract*—We present a 8.7 mm × 10 mm fully-passive brain implant, capable of wireless acquisition of neuropotentials down to 20 μV_{pp}, viz. 3 times lower than before. The implant receives a 2.4 GHz carrier signal from the external interrogator, and mixes it with the neurosignals having a frequency of f_{neuro}. The mixing products (4.8 GHz ± f_{neuro}) are then transmitted back to the external interrogator, and further demodulated to retrieve f_{neuro}. Previous work demonstrated a 15 mm × 16 mm wireless and fully-passive brain implant, capable of detecting emulated neuropotentials as low as 63 μV_{pp}. In this Letter, we present a new neurosensing system, with the following improved features: a) 63% smaller implant, b) 98% smaller interrogator antenna, c) compliance with the strictest FCC standards for patient safety, d) elimination of lumped components within the implant to preserve biocompatibility, and e) 3 times sensitivity improvement. This high sensitivity implies reading of most neural signals generated by the human brain.**

***Index Terms*—Brain implant, miniaturization, neurosensing, passive, sub-harmonic mixing, wireless medical telemetry.**

I. Introduction

BRAIN implant technology can greatly enhance the individual's physical and mental well-being. Possible applications include: detection and interruption of early epileptic seizures, behavioral studies to determine levels of consciousness, understanding and improving the brain's functionality for patients with Alzheimer's, etc. [1], [2].

Existing implanted neuropotential recorders are hindered by several concerns. Specifically, wires are often used to link the brain implants to external recording units [2]. These tethered connections imply severe restrictions to the patient's movements, and limit brain clinical research to static environments. This concern was recently addressed with the advent of wireless brain implants. Nevertheless, these implants use batteries and/or energy harvesters [3], and therefore generate heat. The resulting temperature increase might damage cerebral tissues, eventually disrupting normal brain operation [4]. In [5], an implanted brain recorder with battery placed externally to the skull was presented. Though the recorder transmitted the collected neural data wirelessly to an external receiver, it still protruded outside the skull, making it obtrusive and incurring high risk of infections.

TABLE I
VOLTAGE AND FREQUENCY RANGE OF SIGNALS GENERATED BY THE HUMAN BRAIN [9]

Neural Signals	Voltage Range	Frequency Range
Local Field Potentials / ElectroCorticographic signals	20 – 2000 μV_{pp}	10 – 200 Hz
Neural "spikes"	100 μV_{pp}	300 Hz – 5 kHz

To address these concerns, we recently introduced a new class of wireless fully-passive brain implants (no battery, no energy harvester) [6]-[8]. Our latest work [8] demonstrated a 15 mm × 16 mm brain implant, capable of detecting emulated neuropotentials as low as 63 μV_{pp}. This was done using an external spiral interrogator antenna, 145 mm in diameter. However, to detect all neural signals generated by the human brain (see Table I [9]), we must detect signals down to 20 μV_{pp}. Also, for unobtrusive operation, the implant and interrogator antenna size must be reduced. Notably, we are envisioning integration of the external interrogator into a typical baseball cap or head band.

In this paper, we build on our previous work [8] to design a wireless and fully-passive neurosensing system with the following improved features: a) 63% smaller implant, b) 98% smaller interrogator antenna, c) compliance with even the strictest FCC standards for patient safety, d) elimination of lumped components within the implant to preserve biocompatibility, and e) 3 times sensitivity improvement. For the first time, emulated neuropotentials can be read down to 20 μV_{pp} in a wireless and fully-passive manner. This was achieved by: a) a new set of implanted and interrogator antennas, b) better matching between the implanted antenna and mixer, and c) smaller distance between the implanted and interrogator antennas. This high sensitivity brings forward transformational possibilities for several neural recording applications.

II. Neurosensing System

A. Overview

Fig. 1 shows a block diagram of the proposed neurosensing system. It consists of: (a) the implanted sensor to be placed

Manuscript received March 1, 2016, revised June 06, 2016, accepted July 22, 2016. This material is based upon work supported by the National Science Foundation under Grant No. 1344825.

C. W. L. Lee, A. Kiourti, and J. L. Volakis are with the ElectroScience Laboratory, Department of Electrical & Computer Engineering, The Ohio State University, Columbus, OH 43212 USA (e-mail: lee.6256@osu.edu; kiourti.1@osu.edu; volakis.1@osu.edu).

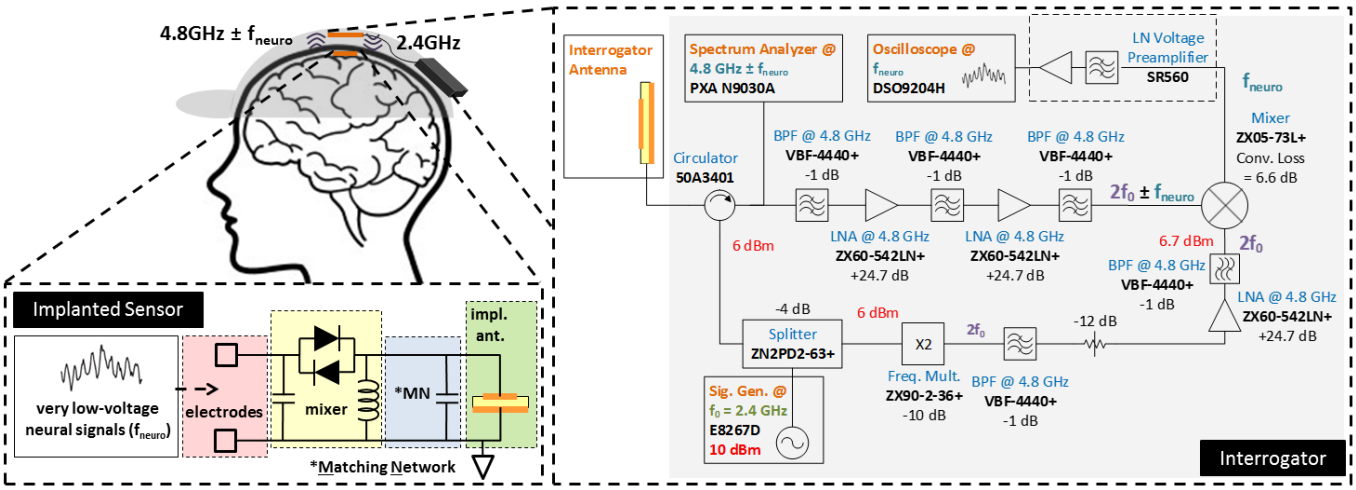

Fig. 1. Neurosensing system block diagram.

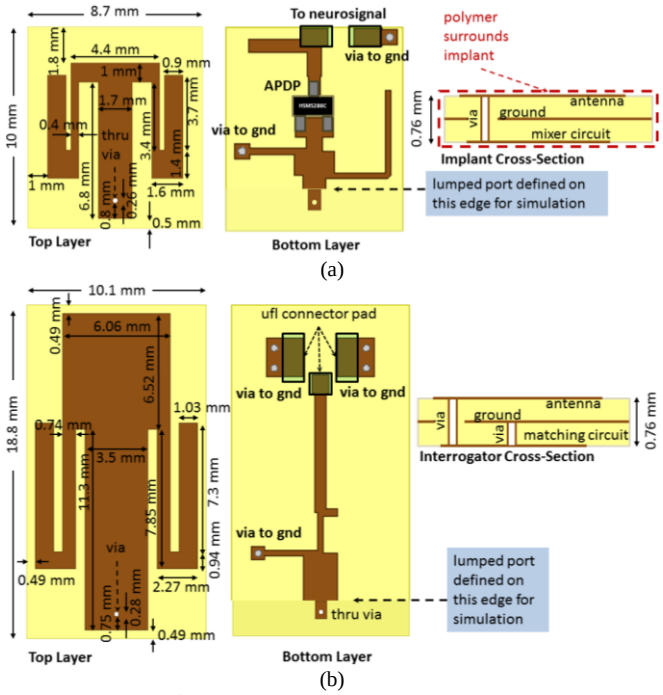

Fig. 2. Layout of antennas employed in the proposed neurosensing system. (a) Implanted antenna. (b) Interrogator antenna.

just under the scalp with the recording electrodes penetrating through the bone and into the brain, and (b) the external interrogator placed right outside the scalp. For comparison, the implant and electrodes in [8] were placed ~12 mm under the skin surface, right beneath the bone layer.

The operation of our neurosensing system has been described in [7]. In brief, the interrogator sends a 2.4 GHz carrier signal to the implanted sensor. Mixing occurs within the implant generating a 4.8 GHz $\pm$ f_{neuro} return signal for detection and signal recovery (f_{neuro} = frequency of the detected neuropotentials). For mixing, we employed an anti-parallel diode pair (APDP) mixer within the implant. The unique operation of this APDP mixer was described in [7].

In this work, we focus on designing a miniaturized brain implant and exterior interrogator antenna that can detect neuropotentials as low as 20 μV_{pp}, viz. 3 times lower than [8]. Specifically, the minimum detectable neurosignal can be calculated as:

$$MDS_{neuro}[\text{dBm}] = Receiver\ Sensitivity[\text{dBm}] + L_{sys}[\text{dB}] \quad (1)$$

where L_{sys} is the transceiver loss. For the employed interrogator, sensitivity is -120 dBm [8]. Thus, to read 20 μV_{pp} (or -90 dBm), L_{sys} must be smaller than 30 dB. We note that:

$$L_{sys}[\text{dB}] = L_{conv}[\text{dB}] + L_{prop}[\text{dB}] + L_{match}[\text{dB}] \quad (2)$$

where L_{conv} is the implanted mixer conversion loss, L_{prop} is the propagation loss (or $|S_{12}|_{dB}$) at 4.8 GHz, and L_{match} is the mismatch loss between the implanted antenna and mixer. To ensure that $L_{sys} < 30$ dB, we must minimize L_{conv}, L_{prop} and L_{match}.

B. Antennas

The goal for the implanted/interrogator antenna system is to achieve efficient radiation at 2.4 GHz and 4.8 GHz $\pm$ f_{neuro}. Low losses at 2.4 GHz imply that smaller carrier power levels are needed to turn "on" the implanted mixer. In doing so, specific absorption rates (SAR) in the surrounding tissues are also reduced. Likewise, low losses at 4.8 GHz $\pm$ f_{neuro} decrease the overall system loss (see Eq. (1)) and hence, improve the minimum detectable neuropotentials.

The proposed implanted antenna is a modified E-shaped dual-band (2.4/4.8 GHz) patch antenna, depicted in Fig. 2(a). It has a footprint of 8.7 mm × 10 mm, viz. 63% smaller than [8]. This remarkable miniaturization was achieved by: a) employing a higher permittivity substrate material, i.e., Rogers TMM13i ($\epsilon_r = 12.2, \tan\delta = 0.0019$) vs. FR-4 ($\varepsilon_r$ = 4.6, tanδ = 0.016) [8], and b) meandering the arms of our former traditional E-shaped patch antenna. Open- and short-circuited stubs were introduced to the back side of the antenna, matching the two frequencies (2.4/4.8 GHz) to the implanted mixer impedance. To ensure biocompatibility, the antenna was coated with a layer of Polydimethylsiloxane (PDMS, $\epsilon_r = 2.8, \tan\delta = 0.001$ [8]) of thickness 0.7 mm. This relatively

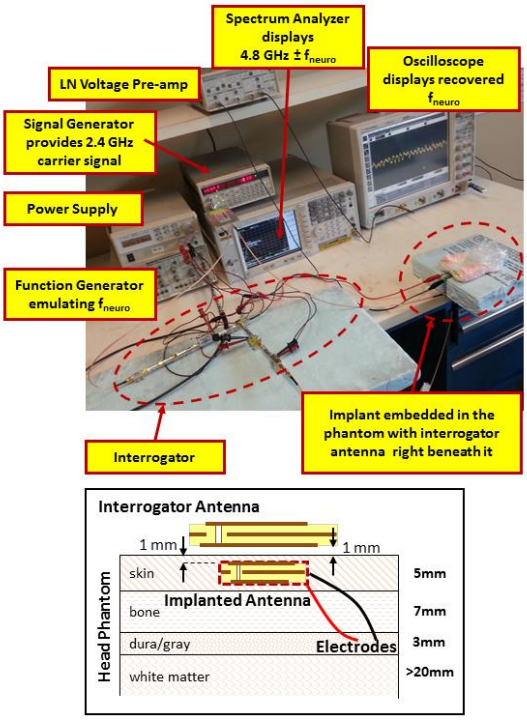

Fig. 3. Measurement setup with the layered head phantom.

lossless layer also decreases the power absorbed by the human tissue, thereby increasing antenna efficiency [10]. The developed interrogator antenna is also a dual-band (2.4/4.8 GHz) E-shaped patch antenna. It has a footprint of 10.1 mm × 18.8 mm, viz. 98% smaller than that in [8], and is depicted in Fig. 2(b). Rogers TMM13i ($\epsilon_r = 12.2, \tan\delta = 0.0019$) was used as the substrate material. As done for the implant, open- and a short-circuited stubs were introduced to the back side of the antenna, matching the two frequencies (2.4/4.8 GHz) to 50 Ω (see Fig. 2(b)).

As shown in Fig. 2, the implanted and interrogator antennas have a 3-layer metallization structure. The radiating patch for each of these resides on top of the two substrate layers, each 15-mil thick. The ground resides in the middle metallization layer, and the matching/mixer circuits are printed on the bottom metallization layer. As usual, to connect the layers, via holes are used.

We note that the antenna dimensions were optimized using an in-house genetic algorithm and simulations were carried out using Ansys HFSS and Keysight ADS. To take into account the antenna pair coupling, the exterior antennas were optimized together to achieve the lowest possible transmission loss.

C. Implanted Mixer

The goal for the implanted mixer circuit is to achieve low conversion loss (viz. low L_{conv}). The block diagram shown in Fig. 1 was used for analysis [7]. The mixer consists of: a) an APDP, b) an inductor that provides the path to ground for the low-frequency neuropotentials (f_{neuro}), c) a capacitor that provides the path to ground for the high-frequency carrier (2.4 GHz), and d) a matching circuit that matches the mixer's impedance to that of the implanted antenna.

To reduce losses, in this work, we modified the mixer to match the implanted antenna shown in Fig. 2(a). To do so, we pursued a design that eliminated the lumped elements and replaced them with open- and short-circuited transmission lines (TLs). As such, soldering within the implant is not needed, implying biocompatibility and lower losses. ADS Momentum was employed to verify system performance before fabrication. The final mixer design is shown in Fig. 2(a). A commercial APDP diode (Avago Technologies, HSMS-286C) with good circuit balance was employed for sub-harmonic mixing, viz. diodes and associated parasitics had identical characteristics.

D. Interrogator

At the interrogator, the backscattered signals with frequencies 4.8 GHz ± f_{neuro} can be demodulated and displayed on an oscilloscope (time-domain). A spectrum analyzer may also be used. In brief, the demodulator mixes the received signals with a reference 4.8 GHz source to retrieve the baseband neuropotentials at f_{neuro}.

The employed interrogator is shown in Fig. 1. It is a slightly modified version of the one described in [11]. To improve the final signal-to-noise ratio, multiple stages of filtering and amplification were used. This architecture has a very low noise figure of 3.8 dB.

III. Neurosensing System Measurement

The measurement set-up for the neurosensor is shown in Fig. 3 with the phantom geometry and tissue recipes as given in [8]. The power of the 2.4 GHz carrier signal was set to 6 dBm, viz. 10 dB lower than the power used in [8]. The lower used interrogator power is attributed to the improved transmission coefficient, $|S_{21}|_{dB}$, between the implanted and interrogator antennas.

A. Sensitivity

The system's loss is the difference between the power of the neuropotentials recorded at the implant (f_{neuro}) vs. the power of the mixing products measured at the interrogator (4.8 GHz ± f_{neuro}). It was found that L_{sys} was 28 dB for 10 Hz < f_{neuro} < 5 kHz. Although this system loss differs from simulation by 8 dB, it is still lower than our target system loss of 30 dB, and 10 dB lower than L_{sys} in [8]. From (1), an $L_{sys} = 28$ dB implies that emulated neuropotentials as low as 20 μV_{pp} can be detected in a wireless and fully-passive manner (see Fig. 4).

Fig. 4 presents a comparison of the actual (emulated) neuropotential waveform vs. that retrieved at the interrogator. For the particular example waveforms, the neuropotentials were as low as 20 μV_{pp}. More noise at the higher frequency neuropotentials can be attributed to the pre-amplifier filter bandwidth used at the interrogator. This noise can be suppressed by performing digital filtering, and/or by zooming in to a narrower band of frequencies. Of course, as the voltage levels increase, the received waveforms are not impacted by noise.

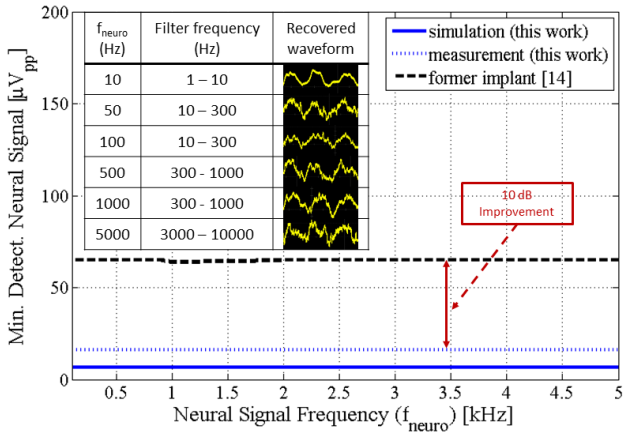

Fig. 4. Minimum detectable neural signal (MDS_{neuro}) with time-domain performance shown in inset.

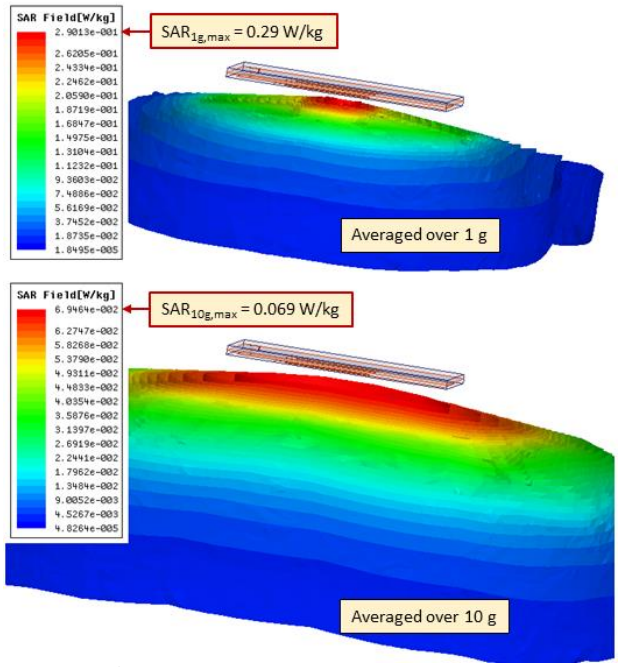

Fig. 5. SAR performance averaged over 1g and 10g with input power at 2.4 GHz set to 6 dBm.

B. Specific Absorption Rate (SAR)

The SAR generated by the proposed neurosensing system was evaluated using Ansys® HFSS. For these studies, we considered a 9-cm-radius spherical head model [12] with each layer's thickness shown in Fig. 3. The brain implant was placed 1 mm below the surface of the skin, and the external interrogator antenna was located 1 mm above the skin. This is depicted in Fig. 5. For calculations, the 2.4 GHz carrier power entering the interrogator antenna was set to 6 dBm. As shown in Fig. 5, the maximum SAR over 1 g of tissue was SAR_{1g} = 0.29 W/kg. When averaged over 10 g of tissue, we found SAR_{10g} = 0.069 W/kg. We note that the Federal Communications Commission (FCC) requires SAR_{1g} < 1.6 W/kg for uncontrolled environment exposure [13], while the International Commission on Non-Ionizing Radiation Protection (ICNIRP) requires SAR_{10g} < 2 W/kg [14]. Thus, the proposed neurosensing system satisfies patient safety requirements set by FCC and ICNIRP [13], [14]. For comparison, our previous implant [8] only satisfied the FCC requirements for controlled environment exposure.

IV. Conclusion

A miniature fully-passive neurosensing system was presented for wireless acquisition of very low power brain signals. Specifically, the proposed system was shown to read emulated neuropotentials down to 20 μV_{pp} at f_{neuro} > 10 Hz. This implies 3 times better sensitivity as compared to previous work [14]. Other features of the proposed system include: a) 63% smaller implant, b) compliance with FCC standards for patient safety, c) 98% smaller interrogator antenna, d) elimination of lumped components within the implant to preserve biocompatibility.

The achieved sensitivity implies reading of most neural signals generated by the human brain in a fully-passive and wireless manner. As such, it brings forward transformational possibilities for several neural recording applications (e.g. epilepsy monitoring and detection, prosthetic control, trauma assessment, etc.).

References

[1] G. Schalk and E.C. Leuthardt, "Brain–computer interfaces using electrocorticographic signals," *IEEE Rev. Biomed*. Eng., vol. 4, pp. 140–154, 2011.
[2] K.D. Wise, "Microelectrodes, microelectronics, and implantable neural microsystems," *Proc. IEEE*, vol. 96, no. 7, pp. 1184–1202, Jul. 2008.
[3] E. Moradi, T. Bjorninen, L. Sydanheimo, J. M. Carmena, J. M. Rabaey, and L. Ukkonen, "Measurement of wireless link for brain–machine interface systems using human–head equivalent liquid," *IEEE Antennas Wireless Propag. Lett.*, vol. 12, pp. 1307–1310, 2013.
[4] S. Kim, P. Thathireddy, R.A. Normann, and F. Solzbacher, "Thermal impact of an active 3-D microelectrode array implanted in the brain," *IEEE Trans. Neural Syst. Rehab. Eng.*, vol. 15, pp. 493–501, 2007.
[5] M. Yin, D.A. Borton, J. Komar, N. Agha, Y. Lu, H. Li, J. Laurens, Y. Lang, Q. Li, C. Bull, L. Larson, D. Rosler, E. Bezard, G. Courtine, A.V. Nurmikko, "Wireless neurosensor for full-spectrum electrophysiology recordings during free behavior," *Neuron.*, vol. 84, pp. 1-13, 2014.
[6] H.N. Schwerdt, W. Xu, S. Shekhar, A. Abbaspour-Tamijani, B.C. Miranda, and J. Chae, "A fully passive wireless microsystem for recording of neuropotentials using RF backscattering methods," *J. Microelectromech. Syst.*, vol. 20, pp. 1119–1130, Oct. 2011.
[7] C.W.L. Lee, A. Kiourti, J. Chae, and J.L. Volakis, "A high-sensitivity fully-passive neurosensing system for wireless brain signal monitoring," *IEEE Trans. Microw. Theory Techn.* vol. 63, no. 6, pp. 2060-2068, Jun. 2015.
[8] A. Kiourti, C.W.L Lee, J. Chae, J.L. Volakis, "A wireless fully-passive neural recording device for unobtrusive neuropotential monitoring," *IEEE Trans. Biomed. Eng.*, vol. 63, no. 1, pp. 131-137, Jan. 2016.
[9] R. R. Harrison, "Design of integrated circuits to observe brain activity," *Proc. IEEE*, vol. 96, no. 7, pp. 1203-1216, Jul. 2008.
[10] F. Merli, B. Fuchs, J. R. Mosig, and A. K. Skrivervik, "The effect of insulating layers on the performance of implanted antennas," *IEEE Trans. Antennas Propag.*, vol. 59, no. 1, pp. 21–31, Jan. 2011.
[11] C.W.L. Lee, A. Kiourti, J. Chae, and J.L. Volakis, "A high-sensitivity fully-passive wireless neurosensing system for unobtrusive brain signal monitoring," *IEEE MTT-S Int. Microw. Symp. Dig*., 2015, pp. 1-4.
[12] J. Kim and Y. Rahmat-Samii, "Implanted antennas inside a human body: Simulations, designs and characterications," *IEEE Trans. Microw. Theory Techn.* vol. 52, no. 8, pp. 1934-1943, Aug. 2005.
[13] Federal Communication Commission (FCC), *Report and order*. FCC96-326.
[14] International Commission on Non-Ionizing Radiation Protection (ICNIRP), "Guidelines for limiting exposure to time-varying electric, magnetic, and electromagnetic fields (up to 300 GHz)," *Health Physics*, vol. 74, no. 4, pp. 494-522, Apr. 1998.